Modeling Chemisorption of Benzene and Its Hydrogenation on Platinum Surfaces. 1. Complexes of Benzene with Pt and Pt_2

Eugene S. Kryachko,*,† Alexei V. Arbuznikov, and Marc F. A. Hendrickx

Department of Chemistry, University of Leuven, Celestijnenlaan 200 F, B-3001 Leuven, Belgium

Received: September 27, 2000; In Final Form: December 12, 2000

The potential energy surfaces (PESs) of the interaction of benzene with Pt and Pt_2 are thoroughly studied at the density functional B3LYP computational level using the Hay−Wadt relativistic core potential. The PES of the benzene−Pt complexation reveals two stable structures, the traditional di-π complex and a σ one which appears to be more stable than the former one by 9.5 kcal/mol. The optimized geometry and vibrational modes of the σ complex are reported in the present work for the first time although it has been predicted experimentally by Gland and Somorjai nearly 30 years ago. We show that the di-$\pi \Leftrightarrow \sigma$ transition is governed by the transition structure with the three-center two-electron bond C···H···Pt. A sliding motion of the Pt atom over the benzene ring to the di-π complex involves a transition structure whose activation barrier amounts 4.7 kcal/mol. The PES of the interaction of bare benzene with Pt_2 consists of three stable structures referred to as di-π, $\pi-\sigma$, and di-σ types. The latter one constitutes a global minimum. The formation of all reported structures is rationalized in terms of molecular orbital patterns.

1. Introduction

The adsorption of aromatic molecules such as benzene on transition-metal surfaces has been a matter of enormous experimental studies in surface science during the last four decades due to the development of transition metal catalysts and the growing technological importance of film−metal interfaces.[1−10] Benzene chemisorption on a platinum−alumina surface in the range of 26−470 °C has been measured in a flow system[1] with observing the two following effects. One of them is a small extent (≤5%) of the reversible adsorption, while the other one is the pressure and temperature independence of extensive irreversible adsorption. Such chemisorption is accompanied by some cracking to C_1-C_4 hydrocarbons at high T and reducing the surface avalaible for a further benzene chemisorption. It has thus been concluded that 0.22 molecules of benzene are chemisorbed/surface Pt atom. With suggestion that benzene fully covers the surface, it has been also estimated that its chemisorption on a (100) face of platinum surface should accommodate 0.185 molecules/surface atom.[1b] In the case of benzene adsorption on the Pt(111) face, this estimation falls to 0.143 (carbon atoms over interstices) or raises to 0.333 (dehydrogenation or distortion to accommodate the carbon skeleton over the interstices). It is interesting, for the purpose of comparison, to mention that physical adsorption of benzene on a monolayer may accommodate 0.166 molecules/surface Pt atom.[1b] However, within a wide range of temperatures, benzene achieves only a low surface coverage.[1b]

It is obvious that an adsorption of any molecule on the atomic surface fully depends on the potential energy surface (PES) of its interaction with the substrate atoms. In the case of benzene adsorbed on the Pt surface, the primary interaction takes place between the π cloud of benzene and the Pt atoms. On the basis of experimental studies, it has been widely accepted that the bonding mechanism strongly involves the substrate d bands accompanied by charge transfer from the π states of benzene to the d bands and, via the donation-back-bonding mechanism, to its π^* orbitals.[2,3] Furthermore, it has been also known experimentally that the chemisorption of benzene on a clean Pt(111) surface is rather strong due to the π-bonding interaction of the aromatic benzene ring with Pt atoms[1−4a−b] and occurs actually via two steps.[4b] The first one is a disordered adsorption of benzene on the platinum surface. In the second step, a surface diffusion orders the adsorbed benzene molecules. The chemisorbed benzene ring appears then lying flat, parallel or nearly parallel to the surface plane[1−4] with the carbon−Pt distance of ∼2.1 Å.[2a] This results in a lower coverage. The benzene chemisorption on Pt(111) is also accompanied by appearance of two observed desorption peaks at 30.8 and 21.0 kcal/mol, respectively.[4a] The activation energy of the dissociation of the C−H bond of benzene on Pt(111) amounts to about 28 kcal/mol.[4a] Also notice that the chemisorption of Bz on a clean Pt(111) surface has been observed up to ca. 400 K. At higher $T > 400$ K, benzene starts to dehydrogenate. Around $T \sim 570$ K, benzene molecules which remain undesorbed lose, on average, three hydrogen atoms.[4a]

Gland and Somorjai[2b] demonstrated a firm experimental evidence of possible $\pi \rightarrow \sigma$ bond transition under adsorption of benzene on Pt surface. Experiments showed that the benzene surface coverage on Pt/Al_2O_3 reaches 0.31.[7a] Such effect was explained by assuming that some C−H bonds of the chemisorbed benzene form nonzero angles with the surface,[3a,7b] and thus, they may be demetalated and interact further with Pt surface. This would likely result in enhancing a surface coverage due to that a certain fraction of adsorbed benzene molecules becomes σ-bonded to the Pt surface.[1a,5c,d,6b] Gland and Somorjai[2b] reported a di-σ-bonded benzene with a multistep formation, in contrast to the formation of the π-bonded benzene occurring via a single-step mechanism.

The other important issue related to the adsorption of benzene on transition-metal surfaces is its hydrogenation to cyclohexane

* Corresponding author. Tel: +32 (16) 32 73 62. Fax: +32 (16) 32 79 92. E-mail: eugene@chem.kuleuven.ac.be.

† On leave from Bogoliubov Institute for Theoretical Physics, Kiev, 03143 Ukraine. E-mail: eugene@bitp.kiev.ua.

10.1021/jp0034933 CCC: $20.00
Published on Web 04/06/2001

C_6H_{12}.[8,9] It is a well-established fact that transition-metal surfaces substantially catalyze the hydrogenation of benzene. Numerous extensive studies have been carried out toward understanding the mechanism of the hydrogenation of benzene on group VIII transition metal catalysts[6b,8] and answering particularly one of the most important questions of whether the gas-phase process $C_6H_6 + 3H_2 \rightarrow C_6H_{12}$ is a structurally sensitive reaction or not? Early studies have identified the benzene hydrogenation on supported Pt catalyst as a facile or structurally insensitive reaction with a specific activity independent of its mode of preparation.[8b] Such conclusion has been corroborated in ref 9c,d. Some anomaly has been however observed in the case of a well-dispersed catalyst, and thus, there likely exist such Pt sites where hydrogen is weakly adsorbed and which become active for the benzene hydrogenation.[8]

Despite the seemingly simple mechanisms of the adsorption of benzene on transition-metal surfaces and of its subsequent hydrogenation, they are still incompletely understood. Such questions as, for example, what are the preferential binding sites of adsorption of benzene on Pt surface, what are the geometries and binding energies of chemisorbed benzene structures, and how does actually the hydrogenation of the chemisorbed benzene occur still remain unanswered.

The present work aims to make a step toward a better understanding of the mechanisms of adsorption of benzene on platinum surfaces and its further hydrogenation. We will rationalize these mechanisms in terms of the molecular orbital (MO) patterns involving the HOMO and LUMO, the highest occupied and the lowest unoccupied MOs, in particular. For this purpose, the present treatment is confined to the modeling of platinum surfaces simply by a single Pt atom and Pt_2 diatomic molecule. This constitutes the key objective of the present part 1. The mechanism of hydrogenation of bare benzene and its subtle features related to its adsorption on Pt surface are studied in a subsequent paper named hereafter as part 2.

We anticipate that the present study provides a clear picture of the elementary steps involving the bond activation and the formation of Bz−Pt complexes, their hydrogenation, and possible reaction intermediates. In the present work, we suggest that benzene molecule is primarily adsorbed on platinum catalyst surface and then becomes hydrogenated. Regarding an appearance of the added hydrogen atoms, it is suggested that there are two different mechanism: (i) The added hydrogen atom is not adsorbed on platinum surface and reacts with the adsorbed benzene, by analogy with Eley-Rideal mechanism.[10] (ii) The added hydrogen is first adsorbed on Pt and then reacts with the adsorbed benzene (the analogue of the Langmuir−Hinshelwood mechanism[10]). We also study the hydrogenation of the adsorbed benzene by subsurface hydrogen atoms (see, e.g., ref 11 and references therein). In conclusion, the key goal of the present study consists of revealing all energetically favorable reaction routes for the hydrogenation of benzene molecules which are adsorbed on Pt.

2. Outline of Computational Framework

2.1. Computational Methodology. All computations were performed at the density functional (DF) hybrid B3LYP computational level making use of the GAUSSIAN 98 package of programs.[12] The Hay−Wadt LanL2DZ relativistic effective core potential (ECP)[13a−c] on the platinum atom was employed. Only the electrons of the outermost core and valence orbitals (5s5p5d6s6p) of Pt were treated explicitly. Spin−orbit coupling was neglected similar to the studies of the ground-state PES of the interaction of Pt with some neutral molecules as, e.g., H_2 and benzene in the neighborhood of stationary points (see ref 14 and references therein). Therefore, the *LS* scheme was applied for further discussion. The Dunning−Huzinaga full double-ς basis set D95(d,p) with polarization functions[13d] was used for the hydrogen and carbon atoms.

Geometries of the studied complexes were fully optimized without any constraint on planarity. Harmonic vibrations were also calculated in order to distinguish the structures of complexes, to analyze further their vibrational spectra, and to obtain the zero-point vibrational energy (ZPVE) for correcting the electronic changes occurring in various reactions. They are retained unscaled. In all calculations of doublet species, the spin contamination was found to be negligible (the expectation value of $\langle S^2 \rangle$ was calculated to be ≤ 0.7502). Throughout the present work, the energy comparison was made in terms of the electronic energy [B3LYP] + ZPVE[B3LYP] energies unless otherwise is notified.

As noticed above, the platinum surface was modeled in the simplest manner by a single platinum atom or by a Pt_2 diatom in order to consider all possible types of bonding with benzene Bz molecule and also to bear in mind that computationally, in particular for locating transition structures which requires a calculation of Hessian matrix, this is a feasible task, even with a quite large basis set. As reference systems for verifying the computational level, the platinum atom, Pt−H diatom, $Pt-H_2$ complex, and bare benzene molecule were chosen, although it is worth mentioning that a remarkable accuracy of the B3LYP level has been recently noticed by Siegbahn and Blomberg.[15] Results of these control calculations are reported in the following section (for recent review see ref 3g).

2.2. Control Calculations of Reference Systems. The ground state of the platinum atom is the triplet state Pt(^{3}D(d^9s^1)) with a $^1S(d^{10}) - {}^3D(d^9s^1)$ splitting that equals 13.14 kcal/mol. This value correlates rather satisfactorily with the experimental values of 11.1 kcal/mol,[16a] 17.56 kcal/mol (with including spin−orbit effects), and 11.02 kcal/mol (after the average over *j* states)[16b] and previous estimations ranging from 9.2 to 26.3 kcal/mol (see Table 4

in refs 16c and 14a). It is interesting to notice that many DF-type potentials such as LSDA, BLYP, BPW91, and B3PW91 employed in conjuction with the Hay−Wadt ECP basis set underestimate the ^{1}S−^{3}D splitting between 2.63 and 4.69 kcal/mol (see Table 1 in ref 16d). Therefore, one concludes that the chosen computational level rather accurately reproduces the ^{1}S−^{3}D splitting.[16e]

The ground state of the Pt−H diatom was found to be the $^2\Sigma$ state with the equilibrium distance $r_e = 1.5231$ Å and the dissociation energy $D_e = 78.196$ kcal/mol relative to the Pt(^{3}D) + H(^{2}S) dissociation limit. This agrees rather satisfactorily with early theoretical estimates of $r_e = 1.47-1.64$ Å (also 1.54 Å[17a] and 1.512 Å[17b]) and its experimentally determined value of $r_e^{expt} = 1.52$ Å[17a] and $D_e = 55.81-89.71$ kcal/mol (see Tables 4 and 5

in ref 16c). The ground-state dipole moment of the PtH diatom is equal to 1.27 D (1.355 D[17a]), and its Pt−H stretching vibrational mode is placed at 2362 cm^{-1} (2299 cm^{-1};[17a] 2314 cm^{-1} via using MRD-CI and 2293 cm^{-1} via using AIMP MRD-CI[17b]). Regarding the ground-state hydrogen molecule, the present computational level predicts the equilibrium distance r_e(H−H) equal to 0.7428 Å with the bond energy of 4.61 eV. The vibrational frequency ν_{H-H} becomes equal to 4485 cm^{-1}. Altogether, our estimates are in a rather good agreement with the experimental data, viz., r_e^{expt}(H−H) = 0.7414 Å, the bond energy of 4.476 eV, and $\nu_{H-H} = 4400$ cm^{-1}.[16a]

The $^1A_1$ ground state of the PtH_2 molecule has a bent geometry characterized by a Pt−H equilibrium distance of 1.5120 Å (1.55/1.52 Å; also 1.52 Å[14b]) and a H−Pt−H bond angle of 85.5° (87.0/85.1°; also 88° in ref 14b) which compare very well to the CASSCF/CI results[18a] given in parentheses. This implies that the most energetically favorable reaction channel of attacking of H_2 by Pt is that when the platinum atom approaches the midpoint of the H−H bond. It further intrudes into the H−H bond and produces its cleavage by moving the hydrogen atoms apart from each other to 2.052 Å which simply means the complete dissociation of the hydrogen molecule. The binding energy of the ground-state of the PtH_2 molecule amounts to 49.26 kcal/mol with respect to the dissociation limit Pt(^{3}D) + H_2($^1\Sigma^+$) that satisfactorily correlates with the theoretical estimate of 40 [18b] and 50 kcal/mol.[14b]

To this end, it is worth comparing the present results with the other DF-type calculations carried out using LSDA, BLYP, BPW91, B3LYP, and B3PW91 in combination with a Hay−Wadt ECP basis on Pt and a 6-31G(d,p) basis set on H. All of them predict a comparable Pt−H equilibrium distance equal to 1.50 Å for LSDA, B3PW91 and 1.52 Å for BLYP and a comparable bond angle ∠H−Pt−H = 84.6° (LSDA) and 86.4° (BLYP). However, the predicted binding energies equal to 84.93 kcal/mol (LSDA), 61.96 kcal/mol (BPW91), 57.45 kcal/mol (BLYP), and 56.95 kcal/mol (B3PW91) taken with respect to the Pt(^{1}S) + H_2 dissociation limit are severely overestimated.[16d] The B3LYP binding energy reported in ref 16d is found to be 52.57 kcal/mol.[16e] The three vibrational modes of the ground-state PtH_2 molecule are calculated at 818, 2405, and 2461 cm^{-1}. The former one is assigned to the scissor vibration while the other two modes to the symmetric and asymmetric stretching vibrations of the Pt−H bonds.

The ground-state benzene molecule of the point symmetry group D_{6h} was characterized by the equilibrium C−C and C−H bond lengths of 1.4029 and 1.0885 Å, respectively. They are both slightly overestimated, by ≈0.0027 and ≈0.0018 Å compared with the recent second-order Møller−Plessett perturbation theory MP2/6-31+G(d,p) (1.400 and 1.0867 Å),[19a] density functional B3LYP/6-311G(d,p) (1.3939 and 1.0844 Å),[19b] and the latest experimental findings (1.3902 ± 0.0002 and 1.0862 ± 0.0015 Å).[19c] On the other hand, they are underestimated in comparison with the B3LYP/6-31G(d,p) computational level[19b] giving the values for the C−C and C−H bond lengths equal to 1.4044 and 1.0952 Å, respectively.

The following sections deal with Bz−Pt and Bz−Pt_2 complexes. In the latter ones, the Pt−Pt distance was frozen at the bulk value of 2.775 Å corresponding to the Pt(111) surface. At this Pt−Pt distance, the lowest state of the Pt_2 diatomic molecule is the triplet with the energy of −238.217 922 hartree, which is larger than the sum of the energies of the two Pt(^{3}D) atoms by 39.10 kcal/mol. The lowest quintet state is located 15.33 kcal/mol above the lowest triplet one. The lowest singlet state of Pt_2 is separated from the lowest triplet one by 27.46 kcal/mol. Its optimization lowers the energy by only 0.65 kcal/mol and shrinks the Pt−Pt distance to 2.687 Å.

3. Benzene−$Pt_{1\le n\le 2}$ Complexes. The present study of the PES of the interaction of bare benzene with the Pt atom reveals two distinct complexes **I** and **II** depicted in Figure 1. Complex **I** is in fact the traditional di-π complex[1−4,20] where a benzene molecule is weakly bound to the Pt atom through the electron density of its π bond. On the contrary, complex **II** has the σ configuration which has not been found theoretically so far although, as mentioned in the Introduction, it has been predicted experimentally by Gland and Somorjai[2b]. Complex **I** is formed

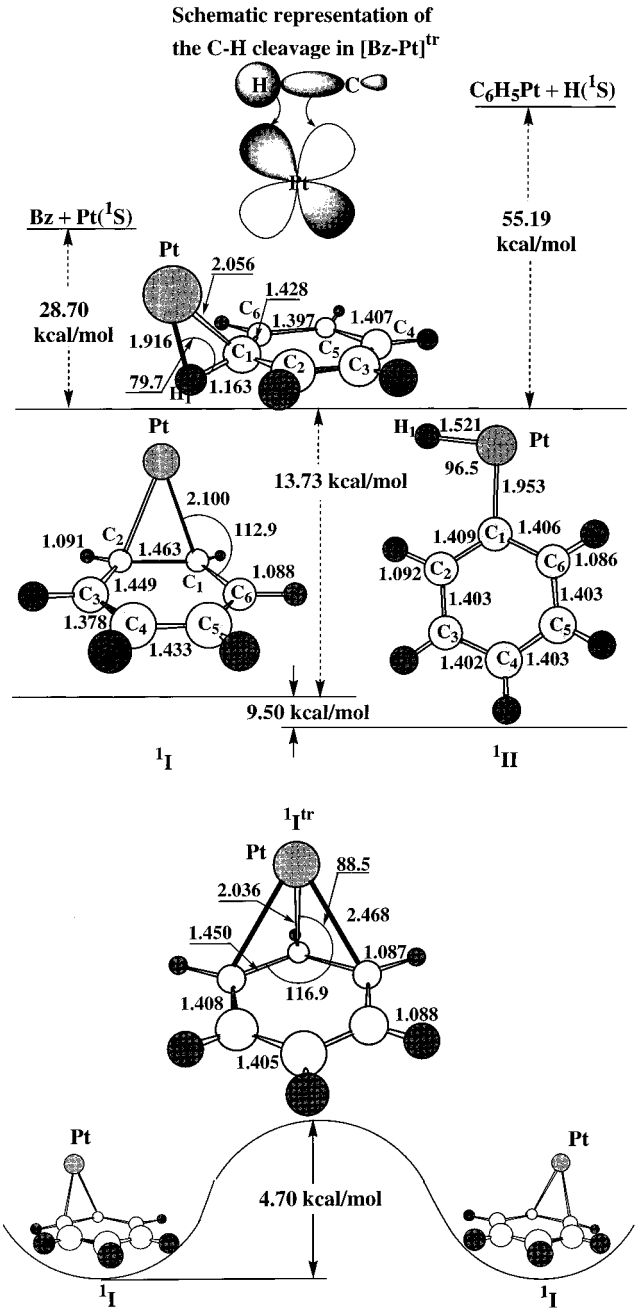

Figure 1. Sections of the PES of the interaction of benzene with the Pt atom. Bond lengths are in Å, and bond angles, in deg. Dashed arrows indicate the unscaled relative energy differences.

when the Pt atom attacks bare benzene perpendicular to its plane, while the formation of complex **II** proceeds in the collinear reaction channel. The transition structure [Bz−Pt]^{tr} with the total dipole moment of 1.94 D whose existence has been also predicted by Gland and Somorjai[2b] governs the di-$\pi \Leftrightarrow \sigma$ bond transition.

The theoretical structure of [Bz−Pt]^{tr} shown in Figure 1 is reported in the present work for the first time. It bifurcates the PES of the Bz−Pt interaction into two reaction channels. One reaction channel with the attacking angle θ ranging the interval $90^o \le \theta < \theta_o$ leads to the direct formation of the Bz−Pt complex **I**. The other one with $\theta_o < \theta \le 180°$ leads to the formation of the Bz−Pt complex **II**. The second channel involves the metalation of an aromatic C−H bond of benzene taking place in [Bz−Pt]^{tr}. The angle θ_o corresponding to the angle ∠PtC_1C_4 in the transition structure amounts to 136.8°

(Figure 1). $[Bz-Pt]^{tr}$ links two dissociation limits, viz., the C_6H_5-Pt + H(^{1}S) and Bz + Pt(^{1}S) shown in Figure 1. The former one refers to the metalation of the C−H bond of benzene with a subsequent removal of a hydrogen atom. With respect to this limit, $[Bz-Pt]^{tr}$ lies below by 55.19 kcal/mol whereas relative to the other one, it is placed below by 28.70 kcal/mol. It is worth mentioning that this value is comparable with the value of ca. 30 kcal/mol found for the C−H activation barrier in the reactions of ethane and methane with Pt and Pd[21] and excellently agrees with the experimental value of the activation energy of the dissociation of the C−H bond of benzene on Pt(111) surface reported by Campbell et al.[4a] (see the Introduction).

In $[Bz-Pt]^{tr}$, the platinum atom "pauses" awaiting for its further insertion into the ortho-aromatic C_1-H bond of benzene and promotes its cleavage shown schematically in Figure 1. This also results in the addition to the unsaturated C_1-C_2 and C_1-C_6 bonds of the length of 1.428 Å. The molecular orbital picture of such C−H cleavage is presented in Figure 1 where it is shown how the d orbital of Pt intrudes the sp C−H bond. Such insertion is accompanied by elongating the C_1-H bond by 0.074 Å compared to benzene and its leaning downward by 23.3° relative to the benzene ring and opposite to the Pt atom. This thus promotes its intermolecular activation. Such bending of the C_1-H bond caused by its partial metalation is described by the imaginary frequency of 129 i cm^{-1} of $[Bz-Pt]^{tr}$. The stretching vibration of the C_1-H bond is predicted at 2421 cm^{-1}. In comparison with the analogous C−H stretching of bare Bz (3176 cm^{-1} [19b]), it is red shifted by 755 cm^{-1} which can be explained by an appearance of a rather strong Pt−H covalent bond. Its juxtaposing with the Pt−H stretching vibration in the ground-state PtH diatom indicates on a blue shift of 59 cm^{-1}.

One may consider the transition structure $[Bz-Pt]^{tr}$ of the Pt−Bz as an example of a complex containing three-center two-electron bond C···H···M[22] which obeys the frequency criteria[22e] of the agostic bond. Namely, in the present case when M = Pt, its frequency is found at 2421 cm^{-1}. Besides, it is a rather short bond with C−H, Pt−C, and Pt−H distances of 1.163, 2.056, and 1.916 Å, respectively. The latter covalent bond is longer by 0.393 Å than the bond length in the PtH($^2\Sigma$) diatomic molecule. The Pt−C bond length is slightly longer, by 0.07 Å, compared to that in the C_6H_5Pt complex. For a further comparison, it is worth noticing that the C···H···Pt bond is substantially bent: $\angle C-H-Pt = 79.7°$.

The HOMO-n ($0 \le n \le 3$) and LUMO of the complex $[Bz-Pt]^{tr}$ and their orbital energies are shown in Figure 2. Numbering of MOs follows their orbital energies. Decomposition of MOs into atomic orbitals (AOs) of bare benzene and Pt illustrates the extent of the metal−ligand mixing and the degree of covalency of the Pt−Bz interaction. The HOMO−LUMO energy gap is equal to 2.44 eV. The MO 27 shows a predominant metal character with a significant contribution of the $5d_{xy}$ and 6s AOs of Pt. The MO 28 lying above MO 27 by 0.24 eV is mainly composed of the σ orbital centered on the carbon atom C_1. It also has a contribution of the 2s AO localized on the bonded hydrogen atom and of the 6s and $5d_{x2-y2}$ AOs of Pt. They both describe the agostic bond in terms of the d AOs of the Pt atom. The MO 29 and HOMO (MO 30) show the dominant metal character due to the large contribution of the 5d AOs of Pt. As seen in Figure 2, the major contribution to the LUMO (MO 31) comes from the 6s orbital of the metal.

3.1. Benzene−Pt Complex I. In the traditional[1−4,20] di-π-adsorbed complex **I** displayed in Figure 1, the Pt atom binds the benzene molecule atop via nearly η^2 bonding to the C═C bond of benzene. Such π-adsorption of Bz has been experimentally observed on a clean Pt(111) surface and can also be realized on the edge of the platinum cluster or on the step edge of the Pt(211) surface. It has been also predicted theoretically by Roszak and Balasubramanian[14c] at the SCF and MP2 computational levels in conjunction with relativistic effective core potentials without spin−orbit coupling (see also ref 3g). The formation of complex **I** can be viewed as the elementary stage toward the completed associative adsorption of Bz on the Pt surface: Bz becomes then oriented parallel to the Pt surface and partially loses its aromaticity due to the alternation of its C−C bonds additonally resulting in the sp^3 hybridization.

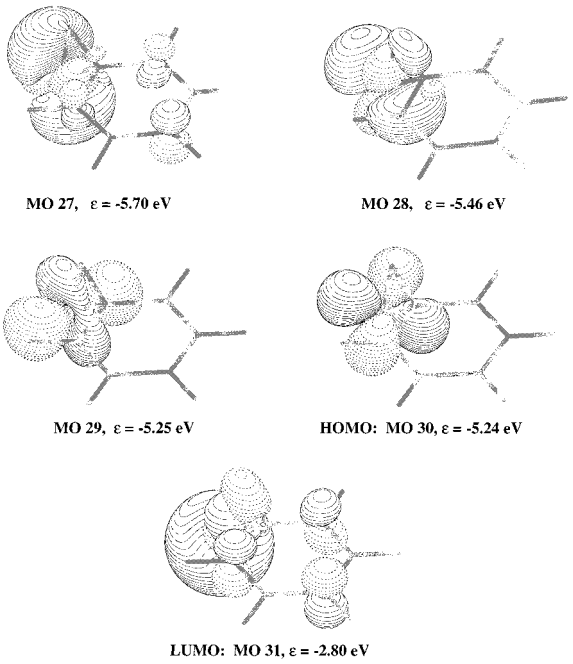

Figure 2. HOMO−LUMO pictorial description of the agostic-bond complex $[Bz-Pt]^{tr}$.

In the present study, we predict the singlet-state di-π complex ^{1}**I** to have a binding energy of 29.3 kcal/mol relative to the limit of the infinitely separated ground-state bare benzene and the Pt(^{3}D) atom. This value of the binding energy agrees satisfactorily with that calculated at the SCF computational level (22 kcal/mol) in ref 14c. Complex ^{1}**I** is separated from the triplet state ^{3}**I** by 72.9 kcal/mol. Comparing with the lowest states of the Pt atom implies that when Bz approaches the Pt atom, the latter undergoes a spin crossing. However, by the analogy with the PtH($^2\Sigma$) diatom, complex ^{1}**I** dissociates straightforwardly to the Bz + Pt(^{1}S) asymptote. With respect to the transition structure $[Bz-Pt]^{tr}$, the energy of the complex ^{1}**I** is lower by 13.73 kcal/mol.

In complex ^{1}**I**, the Pt atom forms two Pt−C bonds of 2.100 Å with the adjacent carbon atoms C_1 and C_2 of Bz moving them apart from each other by the distance of 0.060 Å compared to the equilibrium C−C bond length in bare Bz. The second-neighbor C−C distances also undergo some elongation by ≈0.046 Å whereas the third-neighbor bonds appear to be shorter by ca. 0.025 Å. Two hydrogen atoms adjacent to the Pt−C bonds are slightly elongated by 0.003 Å and lean out of the benzene ring by 10.7°. The Pt atom is placed nearly perpendicular to the Bz ring forming the angle $\angle PtC_2C_4$ of 92.6°.

In terms of Mulliken charges, the formation of such a di-π-bonded complex ^{1}**I** is accompanied by a simultaneous flow of the negative charge of 0.03 e from the second-neighbor carbon atoms and of 0.06 e from the platinum atom to the π-bonded carbon atoms. Some characteristic MOs of the complex ^{1}**I**,

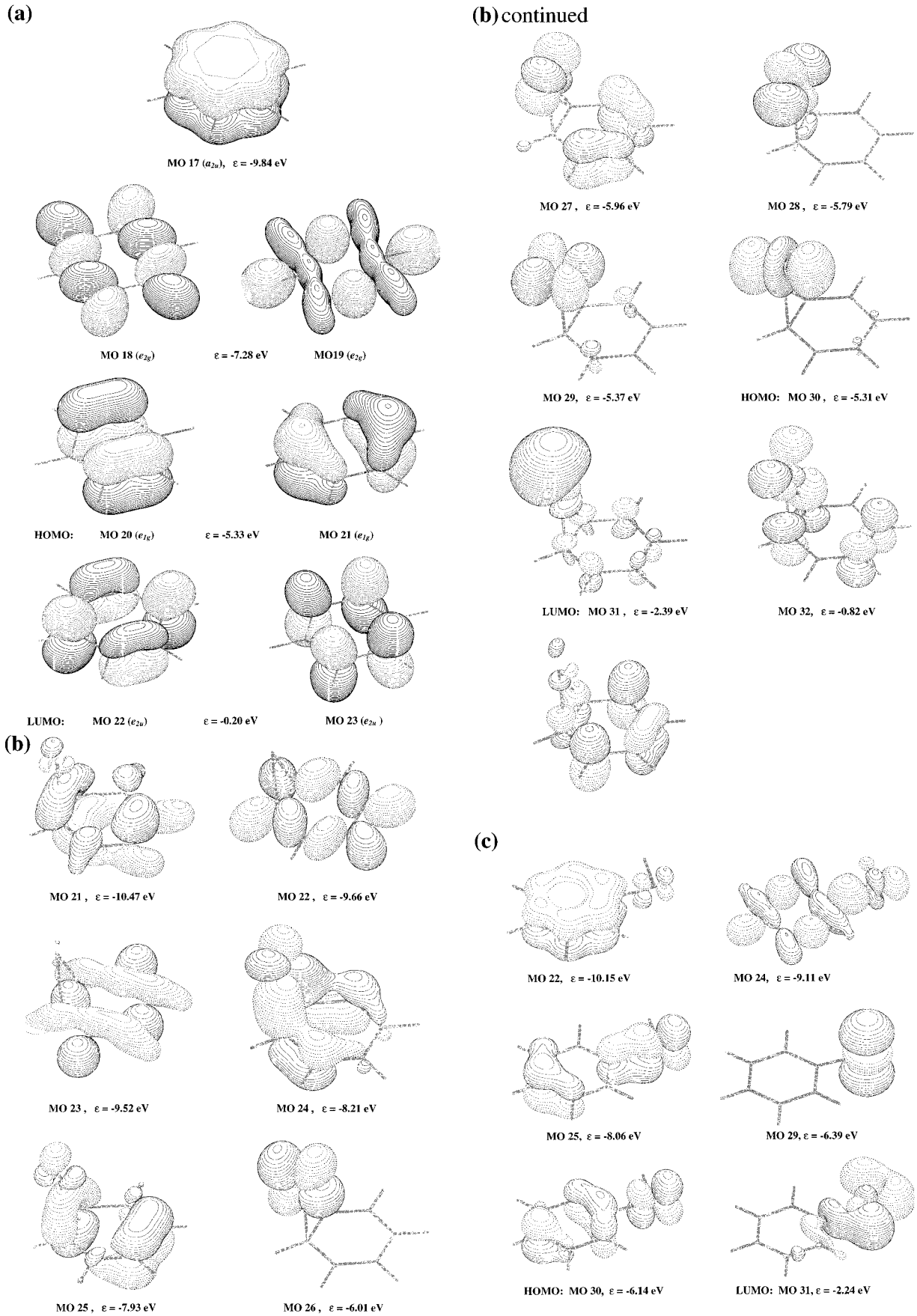

Figure 3. Characteristic MOs, including HOMO and LUMO, of bare benzene (a) and Pt−Bz complexes ^{1}**I** (b) and ^{1}**II** (c). The contour value is 0.055.

including its MO 29, HOMO (MO 30), and LUMO (MO 31), are portrayed in Figure 3b where, for the purpose of comparison, the corresponding MOs of bare benzene are given in Figure 3a. They are formed from the valence 5d, 6s, and 6p AOs of

the Pt atom and from $a_{2u}(\pi)$, $e_{2g}(\sigma)$, $e_{1g}(\pi)$, and $e_{2u}(\pi)$ MOs of benzene. As anticipated, the valence σ orbitals of benzene (MOs 18 and 19 in Figure 3a) are not involved in the interaction with the Pt orbitals and remain nearly unchanged in the complex ^{1}**I** (MOs 22 and 23 in Figure 3b). For this reason, their splitting is rather small, viz., $\leq$0.14 eV. On the contrary, the π orbitals of benzene (MOs 17, 20, and 21 in Figure 3a) are strongly mixed with 5d AOs of Pt, thus giving rise to MOs 21, 24, 25, and 27−30 of the complex ^{1}**I**.

The strongest covalency of the Pt−Bz interaction can be found in the MOs 24, 25, and 27 which are nearly equally contributed from the metal and the ligand. A substantially strong mixing is seen in MO 24 where a noticeable charge is transferred to the d AO of Pt from the π (e_{1g}, MO 21, Figure 3a) orbital of Bz (π donation). The corresponding antibonding counterpart of MO 24, MO 27, is also doubly occupied in the complex ^{1}**I**.

MO 26, higher occupied MOs 28−30, and LUMO (MO 31) show a dominant metal character. For instance, MO 29, with the energy of −5.37 eV nearly equal to that of the degenerate 5d orbitals of Pt(^{1}S), −5.36 eV, is largely composed of the $5d_{yz}$ AO of Pt located on the Pt−C_2 and Pt−C_3 bonds although small contributions of $2p_z$ AOs of the carbon atoms which do not participate in the π-complexation with Pt are seen in Figure 3b as well. Such contributions may be interpreted as an admixture of the π (e_{1g}, MO 21 in Figure 3a) orbital of Bz.

The HOMO (MO 30) of the complex ^{1}**I** lying higher than MO 29 by only 0.06 eV and higher than the HOMO of Bz by 1.52 eV is mainly composed of 6s and 5d AOs of Pt with the predominant 5d character. Its shape resembles the typical d_{z2} orbital. The $2p_x$ AOs of the carbon atoms located on the opposite side of Bz ring relative to Pt make only small contributions to the HOMO. The HOMO−LUMO gap of the complex ^{1}**I** is equal to 2.92 eV. It is smaller compared to that in Bz by a factor of 2.25 and smaller than in Pt which is equal to 6.0 eV. The LUMO (MO 31) shown in Figure 4 is actually a rather strong mixture of Pt and Bz σ character with a predominant contribution from the 6s AO of Pt. The σ contribution of Bz is provided by the $2p_x$ AOs of the carbon atoms. To this end, as demonstrated in Figure 3b, the MO 32 which is separated from the LUMO by 1.57 eV has more substantial contributions from AOs of the carbon atoms and is closer by energy to the next, MO 33. Both these orbitals exhibit a predominant ligand character. Their energy splitting comprises of 0.33 eV only. In fact, MOs 32 and 33 may be considered as the split unoccupied $\pi(e_{2u})$ orbitals of benzene (MOs 22 and 23 in Figure 3a) containing admixtures of 5d and 6p AOs of the Pt atom.

Spectroscopically, the formation of the singlet di-π complex ^{1}**I** manifests in the appearance of the corresponding harmonic Pt−Bz vibrations at 126, 157, 326, and 469 cm^{-1} coupled with the γ(CCC) and δ(CCC) vibrational modes of benzene. Their normal displacement vectors are displayed in Figure 4. Few of them are worth to be discussed. The γ(CCC) vibrational mode of benzene at 714 cm^{-1} which is blue shifted by 7 cm^{-1} in the Pt−Bz complex ^{1}I becomes substantially IR active and describes the asymmetric stretch of the second-neighbor carbon atoms C_1 and C_4 coupled to the symmetric stretches of four other carbon atoms. All ν(C−C) stretching modes of benzene centered at 1356 (b_{2u}), 1499 (e_{1u}), and 1638 (e_{2g}) cm^{-1} are red shifted by 16, 62 and 32, and 88 and 2 cm^{-1}, respectively. Two lower ν(C−H) frequencies at 3149 and 3159 cm^{-1} are assigned to the symmetric and asymmetric C−H stretching vibrations of the carbon atoms C_2 and C_3 which are π-bonded to Pt (Figure 4). In comparison with the C−H stretching vibrations of bare benzene corresponding to the b_{1u} (3176 cm^{-1}) and e_{2g} (3186 cm^{-1}) vibrations modes,[19b] they are shifted both to lower wavenumbers by 27 cm^{-1}. A similar red shift of the C−H stretch of benzene chemisorbed on Pt(111) has been observed experimentally.[23] All degenerate C−H stretching vibrational modes of bare benzene are split due to its chemisorption on the Pt atom. These splittings vary from −27 and −3 cm^{-1} for the e_{1u} irreducible representation of the D_{6h} group and −11 and 2 cm^{-1} for the e_{1u} one.[19b]

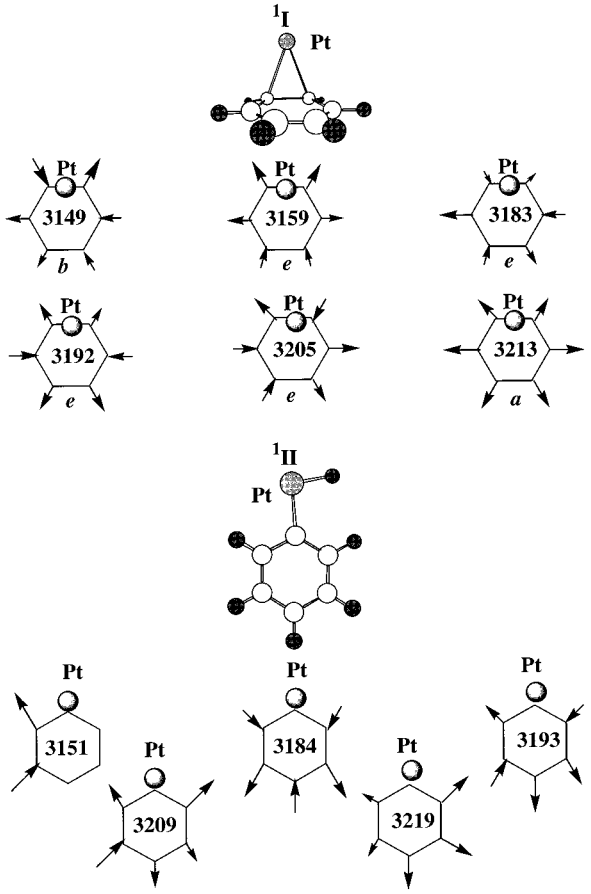

Figure 4. Normal displacements of the harmonic C−H stretching vibrations in the complexes ^{1}**I** and ^{1}**II**. Frequencies are in cm^{-1}.

The di-π adsorbed Bz molecule may undergo a sliding motion over Pt surface via activation of the C−C bond in the vicinity of the platinum atom. This process is governed by the transition structure ^{1}**I**^{tr} which represents itself a tri-π-bonded complex. This complex lies 4.70 kcal/mol above complex ^{1}**I** and is shown in Figure 1. The corresponding Pt−C bond lengths are equal to 2.468, 2.036, and 2.468 Å, respectively. The formation of this tri-π-bonded complex shortens the C−C bond lengths by 0.01 Å. **I**^{tr} is characterized by the imaginary frequency 173 i cm^{-1}.

3.2. Benzene−Pt Complex II. The Bz−Pt complex ^{1}**II** displayed in Figure 1 is more stable than complex ^{1}**I** by 9.5 kcal/mol likely due to the increased donation of the metal 5d AO to the π one of benzene. With respect to the transition structure [Bz−Pt]^{tr}, complex ^{1}**II** is placed below it by 23.25 kcal/mol. The process of the metalation of the C−H bond of benzene is accomplished at this stage giving rise to the σ-aryl−PtH complex being perfectly planar. The platinum atom forms a single σ-bond with the carbon atom C_1 of the bond length equal to 1.953 Å. The latter is shorter than the Pt−C bond length in complex ^{1}**I** and the Pt−C bond length in the σ-aryl−Pt by 0.034 Å. Its inequivalent position with respect to the adjacent carbon atoms caused by the repulsion of the closer hydrogen atoms is demonstrated by the different Pt−C_1–C_2 and Pt−C_1–C_6

bond angles equal to 114.7 and 125.2° and the associated bond lengths of 1.409 and 1.406 Å, respectively. The C_1–Pt–H bond angle is predicted equal to 96.5°, and the Pt–H bond length is predicted equal to 1.521 Å which is only slightly shorter, by 0.002 Å, than in the ground-state PtH diatomic molecule.

Some harmonic vibrational modes of the Pt–Bz complex ^{1}**II** are presented in Figure 4 in order to compare them with the vibrations of bare benzene[19b] and complex ^{1}**I**. First of all, it is worth mentioning that complex ^{1}**II** is characterized by the frequencies 78, 178, and 183 cm^{-1} assigned to the out-of-plane (78 and 178 cm^{-1}) and in-plane (183 cm^{-1}) hindered rotations of the Pt–H bond and the mode at 268 cm^{-1} which describes the Pt–C_1 stretching. Compared to the σ-aryl–Pt complex, the latter frequency is slightly blue shifted by 7 cm^{-1}. Its Pt–H stretching vibration is calculated at 2408 cm^{-1} which is shifted, on one hand, to higher wavenumbers by 46 cm^{-1} compared to the PtH($^2\Sigma$) diatomic molecule and, on the other one, to lower wavenumbers by 13 cm^{-1} if we compare it with that in the transition complex [Bz–Pt]^{tr}. Their normal displacement vectors are depicted in Figure 4.

Some characteristic MOs, including the HOMO and LUMO, of the complex ^{1}**II** are displayed in Figure 3c. Comparing its MO 22 whose orbital energy is equal to −10.15 eV with the MO $17a_{2u}$ of bare benzene whose orbital energy amounts −9.84 eV, we clearly observe the charge transfer from the benzene π cloud to the d AOs of Pt which produces its energy lowering. This is also seen via the comparison of the MO 24 of ^{1}**II** and MO 19 of bare benzene (−9.11 vs −7.28 eV) and, correspondingly, HOMO and MO $21e_{1g}$ (−6.14 vs −5.33 eV). Both these molecular orbitals, MO 24 and HOMO, demonstrate a rather strong mixing of the metal and ligand orbitals. The HOMO of complex ^{1}**II** lies lower than that of complex ^{1}**I** by ca. 1.25 eV. It is mainly attributed by the HOMO of Pt(^{1}S) and the $\pi(e_{1g})$ MO 21 of Bz while the LUMO is actually a strong mixture of the $5d_{x2-y2}$ MO of the platinum atom, orbitals of the terminal hydrogen atom, and the 2s and $2p_y$ AOs on the C_1 carbon atom constituting the σ bonding with Pt. The HOMO–LUMO energy gap amounts to 3.90 eV.

3.3. Benzene–Pt2 Complexes. Three stable complexes **III**–**V** are revealed in the present study of the PES of the interaction of a benzene molecule with Pt_2 (Pt–Pt distance is frozen at the bulky value). Their singlet spin states are found to lie below the triplet ones.

Complex ^{1}**III** shown in Figure 5 originates from the complex ^{1}**I** via forming an additional di-π bond between the carbon atoms of Bz and the second platinum atom. For instance, it illustrates that, on the Pt(111) surface, a bare benzene chemisorbed in such manner lies nearly parallel to the surface. This picture of chemisorption fairly agrees with the experimental findings discussed in the Introduction.

The binding energy of Bz with the Pt_2 cluster amounts to 37.81 kcal/mol. The latter value is larger by 8.52 kcal/mol compared to that of the complex ^{1}**I**. It is obvious that this energy difference is attributed to the formation of a second di-π bond between Bz and the second Pt atom. It is much smaller than the binding energy of the complex ^{1}**I**; i.e., the second di-π bond is much weaker compared to that in the complex ^{1}**I**. As revealed experimentally,[4a,10b] the strong chemisorption of Bz on Pt(111) via a π-bonding interaction produces two desorption peaks with the energies of 30.8 and 21.0 kcal/mol. The former one is in a rather satisfactory agreement with the present model. Relative to the dissociation limit ^{1}**I** + Pt(^{3}D), the binding energy of the complex ^{1}**III** is equal to 47.6 kcal/mol.

It is interesting to make some brief comparison of the geometries of the complexes ^{1}**I** and ^{1}**III**. Instead of the symmetric di-π bonding between Bz and Pt in complex ^{1}**I** with the Pt–C bond length of 2.100 Å, the π–π bonding of Bz to the Pt_2 cluster breaks such symmetry via compressing one Pt–C bond length by 0.053 Å and elongating the other one by 0.142 Å. As seen in Figure 5, the C–C bond adjacent to the carbons bonded to the different Pt atoms is elongated by ∼0.05 Å.

The HOMO–LUMO pictorial representation of the π–π bonding in the complex ^{1}**III** is illustrated in Figure 6. The HOMO–LUMO energy gap comprises 1.94 eV which is lower by nearly 1 eV than that in the complex ^{1}I. The HOMO has a dominant metal character due to large contribution of the antibonding combination of the $5d_{x2-y2}$ AOs. The LUMO also possesses a dominant metal character although the largest contribution is provided by the bonding combination of 6s AOs of the Pt atoms.

The harmonic vibrational modes involving the Pt–Pt diatom are predicted at 59, 85, 164, 195, 238, 365, 508, and 537 cm^{-1}. The former one is assigned to the out-of-plane bending of the Pt–Pt bond coupled to the in-plane deformation of Bz ring. A similar assignment is valid for the vibrational mode at 195 cm^{-1}. The second mode describes the Pt–Pt bending parallel to the benzene ring and the out-of-plane deformation of the latter one. The Pt–Pt stretching vibration is found at the 164 cm^{-1}. The remaining vibrational modes show the dominant character of the out-of-plane motion of the Pt–Pt bond which is strongly coupled to the γ(CCC) modes of benzene. Normal displacements of the C–H stretching vibrations of Bz are illustrated in Figure 5, together with the calculated frequencies. As seen in this figure, the lowest C–H mode found at 3135 cm^{-1} largerly describes the asymmetric stretching vibration of the C_1–H_1 and C_2–H_2 bonds. Its comparison with the b_{1u} C–H stretching mode of bare benzene indicates a red shift of 31 cm^{-1}.

Complex ^{1}**IV** is also depicted in Figure 5. It has a mixed σ–π bonding of Bz to the Pt atoms, and for this reason, its formation may occur via two possible reaction routes. One route starts from the complex ^{1}**II** which binds the second Pt atom via the di-π bonding, similar to the bonding in complex ^{1}**I**. The other one departs from the complex ^{1}**I**: the second Pt atom, being inserted into the C–H bond of Bz, substitutes it and forms the complex ^{1}**IV**. It is obvious that the former reaction route is preferential. On one hand, complex ^{1}**IV** is more stable, by 7.5 kcal/mol, than complex ^{1}**III** due to the bonding interaction of the d orbital of Pt with the σ MO of Bz. On the other hand, compared to the dissociation limit of complex ^{1}**II** + Pt(^{3}D), its binding energy comprises 45.6 kcal/mol which is smaller than the binding energy of complex ^{1}**III** relative to the corresponding limit complex ^{1}**I** + Pt(^{3}D). Besides, along the first reaction route, the formation of the di-σ bonding between Bz and Pt is accompanied by shrinking the σ Pt–H bond length in complex ^{1}**I** by ca. 0.01 Å, elongating the Pt–H bond by ∼0.04 Å, and increasing the C–Pt–H bond angle by ca. 11°. Correspondingly, the Pt–H stretching vibration in complex ^{1}**IV** found at 2208 cm^{-1} undergoes a red shift of 200 cm^{-1}. The Pt–Pt stretch is predicted at 121 cm^{-1} that is lower by 45 cm^{-1} compared to that in the complex ^{1}**III**. The normal displacement vectors of the C–H stretching vibrations are shown in Figure 5. In particular, we notice that the higher C–H vibrational mode found at 3229 cm^{-1}, which is dominantly the coupled symmetric stretches of the C_1–H_1 and C_6–H_6 bonds and corresponds to the a_{1g} C–H stretch of bare benzene, becomes blue shifted by 15 cm^{-1}.

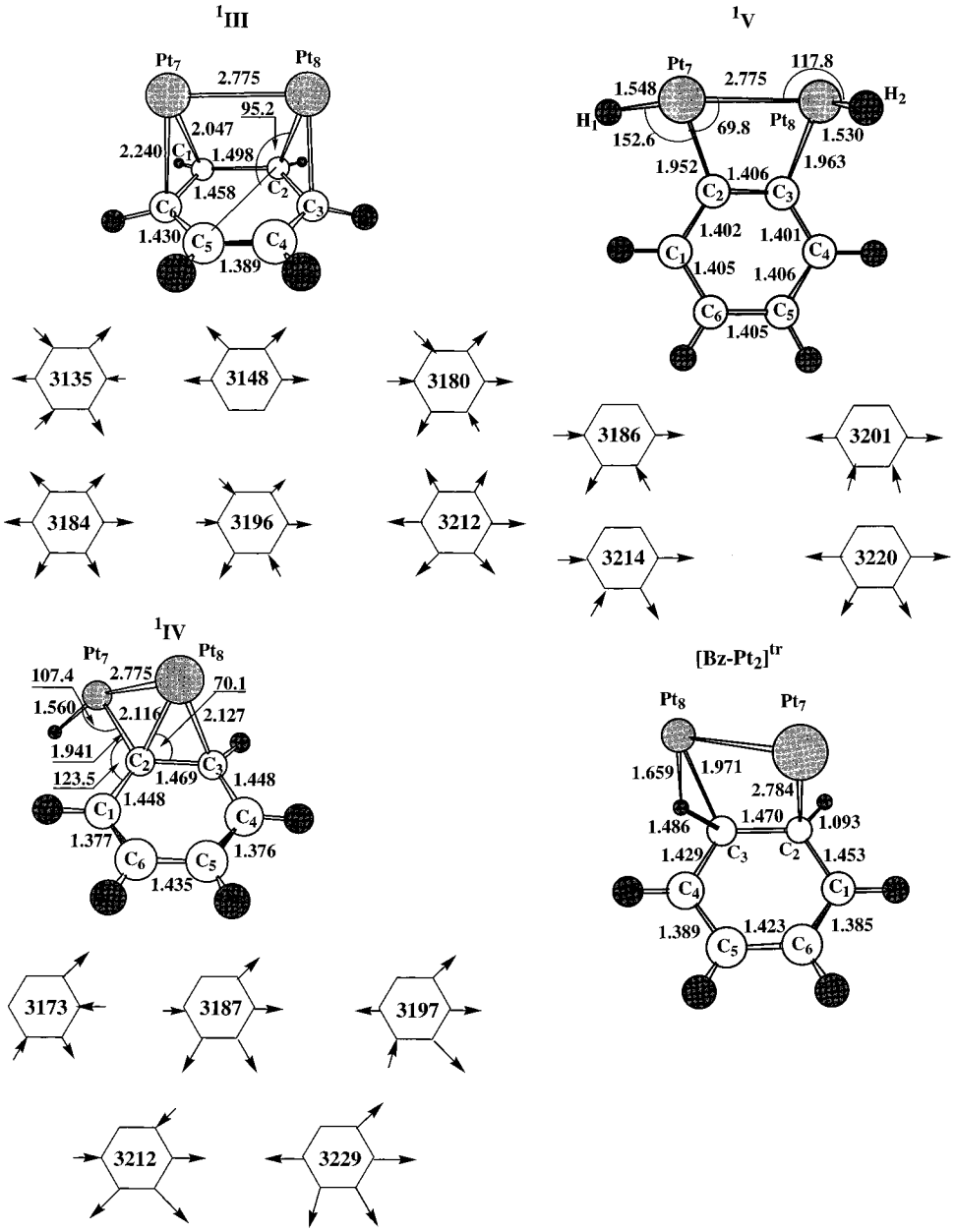

Figure 5. Most stable Pt_2 −Bz complexes ^{1}**III**, ^{1}**IV**, and ^{1}**IV** and their harmonic C−H stretching vibrations. The transition structure $[Bz-Pt_2]^{tr}$ governing the ^{1}**III** ⇔ ^{1}**IV** transition is also displayed. Bond lengths are in Å, and bond angles, in deg. Frequencies are in cm^{-1}.

The HOMO and LUMO of the complex ^{1}**IV** are depicted in Figure 6. Its HOMO−LUMO gap is wider than in the complex ^{1}**III** and equal to 2.88 eV. The HOMO is situated on the Pt diatom with a predominant contribution from a 5d orbital of the Pt atom σ-bonded to Bz. The LUMO is dominantly attributed to the 6s AO of the Pt atom which is di-π-bonded to benzene although some noticeable contribution from π orbitals of Bz are also worth to mention.

Transition ^{1}**III** ⇔ ^{1}**IV** is governed by the transition structure $[Bz-Pt_2]^{tr}$ (Figure 5) with an activation barrier of 28.60 kcal/mol with respect to the $\pi-\pi$ complex ^{1}**III**. It is characterized by the imaginary frequency of 968 i cm^{-1}. $[Bz-Pt_2]^{tr}$ has three-center two-electron bond with the corresponding bond lengths r(Pt−H) = 1.659 Å and r(C−H) = 1.486 Å. The former bond length is smaller by ca. 0.26 Å compared to the corresponding one in the $[Bz-Pt]^{tr}$ transition complex whereas the latter is longer by ca. 0.32 Å.

The global minimum on the PES of the interaction of Bz with Pt_2 is located at the $\sigma-\sigma$ complex ^{1}**V** (Figure 5). Its energy is lower by 16.21 kcal/mol compared to the $\pi-\pi$ complex ^{1}**III**. As shown in Figure 5, two Pt atoms lying in the Bz plane form Pt−H bonds of 1.530 and 1.548 Å long, respectively. In a comparison of the geometries of the $\pi\angle\pi$ and $\sigma\angle\sigma$ complexes, it is worth noticing that the formation of the latter one does not cause any remarkable changes in the intra-ring distances varying in the interval 1.401−1.406 Å. The dihedral angle $\angle H_3Pt_8Pt_7H_2$ is equal to 153.1°.

The symmetric and asymmetric Pt−Pt stretching vibrations in the $\sigma-\sigma$ complex are predicted at 103 and 171 cm^{-1}, respectively. The corresponding Pt−H stretching vibrational frequencies are equal to 2272 cm^{-1} (180 km/mol) and 2354 cm^{-1} (64 km/mol). The former one mainly corresponds to the Pt_7-H_2 bond while the latter to the Pt_8-H_3 one. Both stretching frequencies are red shifted by 136 and 54 cm^{-1} relative to the Pt−H stretching frequency of the complex ^{1}**II**. Four C−H stretching vibrational frequencies of the complex ^{1}**V** are indicated in Figure 5 together with the vectors of their normal displacements. Comparing them with the C−H stretching

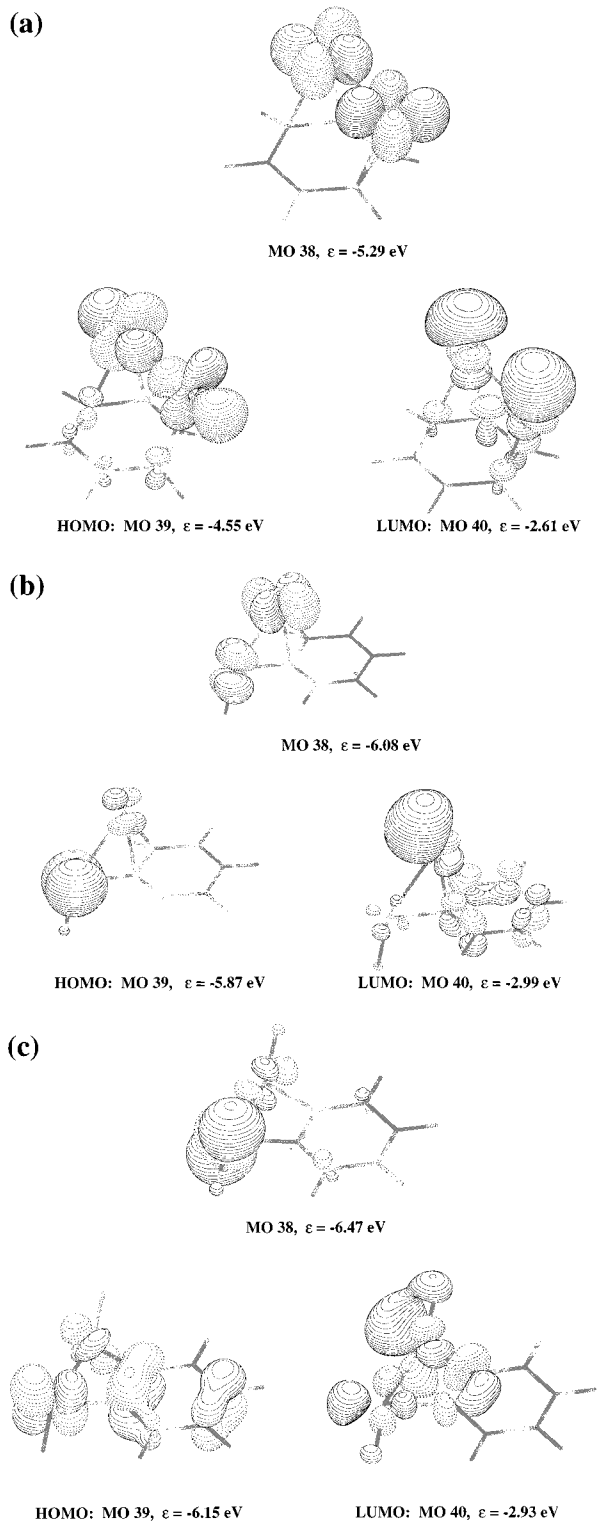

Figure 6. HOMO-1, HOMO, and LUMO of the complexes ^{1}**III** (a), ^{1}**IV** (b), and ^{1}**V** (c) (contour spacing 0.055). ϵ indicates the orbital energy in eV.

vibrations of bare benzene, we conclude that two first vibrations at 3186 and 3201 cm^{-1} correspond to the e_{2g} stretch of bare benzene, the third one at 3214 cm^{-1} to the e_{1u}, and, finally, the fourth mode predicted at 3220 cm^{-1} to the a_{1g} stretch.[19b]

The HOMO and LUMO of the complex ^{1}**V** are presented in Figure 5. Among three Bz−Pt_2 complexes studied in the present work, complex ^{1}**V** is characterized by the widest HOMO−LUMO gap equal to 3.22 eV. The HOMO is the result of a π interaction between the bonding combination of 5d AOs on the Pt atoms and π (e_{1g}, MO 21 in Figure 3a) orbital of the benzene. The contributions of the AOs of the Pt diatom and Bz are comparable, and their interaction is realized in an antibonding manner. Like the HOMO, the LUMO also has an antibonding nature as a result of the interaction of the orbitals of the Pt diatom with σ orbitals of benzene. It is worth noticing that a rather small distortion of the geometry of the complex ^{1}**V**, manifested in that the Pt−C bond lengths differ only by 0.011 Å, causes a significant deformation of the electron cloud.

Summarizing, we reveal that there exist at least three possibile routes for the chemisorption of Bz on a platinum surface. Among them, the favorable one is the edge-type chemisorption leading to the formation of the complex ^{1}**V** where each Pt atom substitutes the C−H bond by a C−Pt bond and becomes also bonded to the "loose" hydrogen atom of Bz. However, its formation is highly unlikely on clean Pt(111) surfaces where chemisorption occurs primarily via the formation of the $\pi-\pi$ complex ^{1}**III**.

4. Summary and Conclusions

We have thoroughly investigated the characteristic sections of the PESs of the interaction of a benzene molecule with a Pt atom and a Pt_2 diatom. The PES of the benzene−Pt interaction consists of two stable minimum energy structures one of which is actually the traditional di-π complex ^{1}**I**. We have revealed that it is formed when a benzene molecule attacks the Pt surface nearly perpendicular to its ring plane. The other, collinear reaction route leads to the formation of the σ complex ^{1}**II**. On one hand, it appears to be more stable by 9.5 kcal/mol than the di-π complex. On the other hand, its formation, although experimentally predicted by Gland and Somorjai[2b] nearly 30 years ago, is not straightforward as in the case with the di-π complexation. In fact it requires a passage throughout the transition structure $[Bz-Pt]^{tr}$ which necessarily involves the platination of the aromatic C−H bond of benzene occurring via the formation of three-center two-electron C···H···Pt bond which can be apparently referred to an agostic bond. That is why, under real reaction conditions, it is unlikely energetically preferable although its accommodation on the Pt surface requires less space compared to that needed for the di-π complex.

The aforementioned transition structure with the agostic bond has been reported in the present study for the first time, and it will be interesting to detect such a structure experimentally. For this purpose, we have presented its C−H stretching vibrational modes which might be useful as "fingerprints". This PES also includes the transition structure governing the sliding motion of benzene over Pt surface. It proceeds via activation of the C−H bond in the vicinity of the Pt atom, and due to a low activation barrier of 4.7 kcal/mol, is energetically accessible.

The PES of the Bz−Pt_2 interaction is composed of three stable minima describing, correspondingly, the di-π, $\sigma-\pi$, and, finally, di-σ complexes. The latter one is the global minimum. Nevertheless, despite the fact that the di-σ complex ^{1}**V** is more stable by 16.2 kcal/mol compared to the di-π complex ^{1}**III**, we stress that, by the analogy with the Pt−Bz PES, the di-π complex is likely the most preferable under real conditions. Rather interestingly, the intermediate $\sigma-\pi$ type complex ^{1}**IV** appears to be more stable than the di-π one by only 7.5 kcal/mol compared to the energy difference of 9.5 kcal/mol between the complexes ^{1}**II** and ^{1}**I**. However, the activation barriers separated them are equal to 28.6 and 23.3 kcal/mol, respectively. Therefore, a likely scenario for the formation of a σ complex emerges as that it forms preferentially at those sites where a benzene molecule is chemisorbed on a single Pt atom. Theoretically predicted

harmonic vibrations of the studied variety of the energy minimum structures of Bz−Pt and Bz−Pt_2 complexes will be rather helpful for analyzing the experimental IR spectra and assigning each vibrational band to a specific structure.[23]

We have rationalized the Pt−Bz and Pt_2−Bz interactions in terms of the population of the MOs and the accompanied charge transfer. In particular, we have shown that the HOMO−LUMO concept provides a rather transparent and useful picture of the formation of all studied complexes of benzene with Pt and Pt_2. Concluding, we anticipate that the present study offers a better understanding of the molecular orbital nature of reactivity in the adsorption of benzene on Pt surfaces and of the variety of reaction profiles accompanying this process.

Acknowledgment. E.S.K. is grateful for a Grant of the University of Leuven and thanks Minh Tho Nguyen for warm hospitality and useful discussions. He also thanks Raman Sumathy for helpful discussions. A.V.A. and M.H. are indebted to the Fund for Scientific Research (FWO-Vlaanderen) and Geconcerteerde Onderzoeksacties (GOA) for financial support. The authors thanks the reviewers for valuable comments and suggestions.

References and Notes

(1) (a) Garnett, J. L. *Catal. Rev.* **1972**, *5*, 229. (b) Moyes, R. B.; Wells, P. B. *Adv. Catal.* **1973**, *23*, 121. (c) Somorjai, G. A. *Annu. Rev. Phys. Chem.* **1994**, *45*, 721.

(2) (a) Ogletree, D. G.; Van Hove, M. A.; Somoraji, G. A. *Surf. Sci.* **1987**, *183*, 1. (b) Gland, J. L.; Somorjai, G. A. *Surf. Sci.* **1973**, *38*, 157. (c) Stair, P. C.; Somorjai, G. A. *J. Chem. Phys.* **1977**, *67*, 4361. (d) Netzer, F. P.; Matthew, J. A. D. *Solid State Commun.* **1979**, *29*, 209. (e) Tsai, M. C.; Muetterties, E. L. *J. Am. Chem. Soc.* **1982**, *104*, 2534. (f) Johnson, A. L.; Muetterties, E. L.; Stohr, J. *J. Am. Chem. Soc.* **1983**, *105*, 7183. (g) Anderson, A. B.; McDevitt, M. R.; Urbach, F. L. *Surf. Sci.* **1984**, *146*, 80.

(3) (a) Abon, M.; Bertolini, J. C.; Billy, J.; Massardier, J.; Tardy, B. *Surf. Sci.* **1985**, *162*, 395. (b) Garfunkel, E. L.; Farias, M. H.; Somorjai, G. A. *J. Am. Chem. Soc.* **1985**, *107*, 349. (c) Mate, C. M.; Somorjai, G. A. *Surf. Sci.* **1985**, *160*, 542. (d) Horsley, J. A.; Stohr, J.; Hitchcock, A. P.; Newbirg, D. C.; Johnson, A. L.; Sette, F. *J. Chem. Phys.* **1985**, *83*, 6099. (e) Abon, M.; Billy, J.; Bertolini, J. C.; Tardy, B. *Surf. Sci.* **1986**, *167*, L187. (f) Somers, J. Bridge, M. E.; Lloyd, D. R.; McCabe, T. *Surf. Sci.* **1987**, *181*, L167. (g) Dedieu, A. *Chem. Rev.* **2000**, *100*, 543.

(4) (a) Campbell, J. M.; Seimanides, S.; Campbell, C. T. *J. Phys. Chem.* **1989**, *93*, 815. (b) Gland, J. L.; Somorjai, G. A. *Surf. Sci.* **1974**, *41*, 387. (c) Nagao, M.; Suda, Y. *Langmuir* **1989**, *5*, 42. (d) Ioannides, T.; Tsapatsis, M.; Koussathana, M.; Verykios, X. E. *J. Catal.* **1995**, *152*, 331. (e) Nyberg, G. L.; Bare, S. R.; Hofmann, P.; King, D. A.; Sorman, M. *Appl. Surf. Sci.* **1985**, *22/23*, 392. (f) Davis, S. M.; Gordon, B. E.; Press, M.; Somorjai, G. A. *J. Vac. Sci. Technol.* **1981**, *19*, 231.

(5) (a) Jing, Z.; Whitten, J. L. *Surf. Sci.* **1991**, *250*, 147. (b) Gomez, R.; Del Angel, G.; Damian, C.; Corro, G. *Kinet. Catal. Lett.* **1979**, *11*, 137. (c) Bandiera, J.; Meriavdeau, P. *Kinet. Catal. Lett.*. **1988**, *37*, 373. (d) Srinivas, S. T.; Rao, P. K. *J. Catal.* **1994**, *148*, 470. (e) Surman, M.; Bare, S. M.; Hofman, P.; King, D. A. *Surf. Sci.* **1983**, *126*, 349. (f) Surman, M.; Bare, S. M.; Hofman, P.; King, D. A. *Surf. Sci.* **1987**, *179*, 243.

(6) (a) Tetenyi, P.; Babernics, L. *J. Catal.* **1963**, *8*, 215. (b) Orozco, J. M.; Webb, J. *Appl. Catal.* **1983**, *6*, 67.

(7) (a) Palazov, A.; Bonev, C.; Shopov, D.; Lietz, G.; Sárkány, A.; Völter, J. *J. Catal.* **1987**, *103*, 249. (b) Koel, B. E.; Crowell, J. E.; Mate, C. M.; Somorjai, G. A. *J. Phys. Chem.* **1984**, *88*, 1988. (c) Friend, C. M.; Muetterties, E. L. *J. Am. Chem. Soc.* **1981**, *103*, 773. (d) Friend, C. M.; Muetterties, E. L. *J. Phys. Chem.* **1982**, *86*, 5067.

(8) (a) Singh, U. K.; Vannice, M. A. *AIChE J.* **1999**, *45*, 1059 and references therein. (b) Rashid, K. K. A.; Lakshmi, K. V.; Nandan, M.; Xavier, K. O.; Sen, B. In *Recent Advances in Basic and Applied Aspects of Industrial Catalysis*; Prasada Rao, T. S. R.; Murali, G., Eds.; Studies in Surface Science and Catalysis, Vol. 113; Elsevier: Amsterdam, 1998; pp 829−834.

(9) (a) Xu, C.; Tsai, Y.-L.; Koel, B. E. *J. Phys. Chem.* **1994**, *98*, 585. (b) Peck, J. W.; Koel, B. E. *J. Am. Chem. Soc.* **1996**, *118*, 2708. (c) Basset, J. M.; Dalmai-Imelik, G.; Primet, M.; Mutin, R. *J. Catal.* **1975**, *37*, 22. (d) Van Meerten, R. Z. C.; Morales, A.; Barbier, J.; Maurel, R. *J. Catal.* **1979**, *58*, 43.

(10) Somorjai, G. A. *Introduction to Surface Chemistry and Calalysis*; Wiley: New York, 1994.

(11) (a) Johnson, A. D.; Daley, S. P.; Utz, A. L.; Ceyer, S. T. *Science* **1994**, *257*, 223. (b) Daley, S. P.; Utz, A. L.; Trautman, T. R.; Ceyer, S. T. *J. Am. Chem. Soc.* **1994**, *116*, 6001.

(12) Frisch, M. J.; Trucks, G. W.; Schlegel, H. B.; Scuseria, G. E.; Robb, M. A.; Cheeseman, J. R.; Zakrzewski, V. G.; Montgomery, J. A., Jr.; Stratmann, R. E.; Burant, J. C.; Dapprich, S.; Millam, J. M.; Daniels, A. D.; Kudin, K. N.; Strain, M. C.; Farkas, O.; Tomasi, J.; Barone, V.; Cossi, M.; Cammi, R.; Mennucci, B.; Pomelli, C.; Adamo, C.; Clifford, S.; Ochterski, J.; Petersson, G. A.; Ayala, P. Y.; Cui, Q.; Morokuma, K.; Malick, D. K.; Rabuck, A. D.; Raghavachari, K.; Foresman, J. B.; Cioslowski, J.; Ortiz, J. V.; Stefanov, B. B.; Liu, G.; Liashenko, A.; Piskorz, P.; Komaromi, I.; Gomperts, R.; Martin, R. L.; Fox, D. J.; Keith, T.; Al-Laham, M. A.; Peng, C. Y.; Nanayakkara, A.; Gonzalez, C.; Challacombe, M.; Gill, P. M. W.; Johnson, B.; Chen, W.; Wong, M. W.; Andres, J. L.; Gonzalez, C.; Head-Gordon, M.; Replogle, E. S.; Pople, J. A. *GAUSSIAN 98*, revision A.5; Gaussian, Inc.: Pittsburgh, PA, 1998.

(13) (a) Hay, P. J.; Wadt, W. R. *J. Chem. Phys.* **1985**, *82*, 270. (b) Wadt, W. R.; Hay, P. J. *J. Chem. Phys.* **1985**, *82*, 284. (c) Hay, P. J.; Wadt, W. R. *J. Chem. Phys.* **1985**, *82*, 299. (d) Dunning, T. H., Jr.; Hay, P. J. In *Modern Theoretical Chemistry*; Schaefer, H. F., III, Ed.; Plenum: New York, 1976; Vol. 3, p 1.

(14) (a) Nakatsuji, H.; Matsuzaki, Y.; Yonezawa, T. *J. Chem. Phys.* **1988**, *88*, 5759. (b) Gropen, O.; Sjøvoll, M.; Strømsnes, H.; Karlsen, E.; Swang, O.; Faegri, K., Jr. *Theor. Chim. Acta* **1994**, *87*, 373. (c) Roszak, S.; Balasubramanian, K. *Chem. Phys. Lett.* **1995**, *234*, 101. (d) Heinemann, C.; Koch, W.; Schwarz, H. *Chem. Phys. Lett.* **1995**, *245*, 509. (e) Kua, J.; Faglioni, F.; Goddard, W. A., III. *J. Am. Chem. Soc.* **2000**, *122*, 2309.

(15) Siegbahn, P. E. M.; Blomberg, M. R. A. *Chem. Rev.* **2000**, *100*, 421.

(16) (a) Huber, K. P.; Herzberg, G. *Molecular Spectra and Molecular Structure Constants of Diatomic Molecules*; Van Nostrand Reinhold: New York, 1979. (b) Moore, C. E. *Atomic Energy Levels As Derived From the Analyses of Optical Spectra*; National Bureau of Standards: Washington, D C, 1971; Vol. III, pp 38−43, 181−185. (c) Gropen, O.; Almlöf, J.; Wahlgren, U. *J. Chem. Phys.* **1992**, *96*, 8363. (d) Diez, R. P. *Chem. Phys. Lett.* **1998**, *287*, 542. (e) The reason of the discrepancy between the present value of the $^1S-^3D$ splitting and that reported for the B3LYP calculation in ref 15d and equal to 3.50 kcal/mol is unclear. That is why we provide the calculated values of the energy of −119.077 816 hartree of the ^3D and the energy of −119.056 878 hartree of the ^1S state of the Pt atom, respectively. The analogous situation takes place with the ground-state PtH_2 molecule which can be partially explained by the different choices of the basis sets. For instance, in ref 15d, the hydrogen atom is described via 6-31G(d,p) basis set.

(17) (a) Balasubramanian, K.; Feng, P. Y. *J. Chem. Phys.* **1990**, *92*, 541. (b) Marian, C. M.; Wahlgren, U. *Chem. Phys. Lett.* **1996**, *251*, 357.

(18) (a) Balasubramanian, K. *J. Chem. Phys.* **1987**, *87*, 2800. (b) Anderson, J. R. *Structure of Metallic Catalysts*; Academic: New York, 1975.

(19) (a) Kryachko, E. S.; Nguyen, M. T. *J. Phys. Chem. A* **2000**, *104*, in press. (b) Palafox, M. A. *Int. J. Quantum Chem.* **2000**, *77*, 661. (c) Plíva, J.; Johns, J. W. C.; Goodman, L. *J. Mol. Spectrosc.* **1991**, *148*, 427.

(20) Tsutsui, M.; Levy, M. N.; Nakamura, A.; Ichikawa, M.; Mori, K. *Introduction to Metal π-Complex Chemistry*; Plenum: New York, 1970.

(21) (a) Blomberg, M. R. A.; Brandemark, U.; Siegbahn, P. E. M. *J. Am. Chem. Soc.* **1983**, *105*, 5557. (b) Blomberg, M. R. A.; Siegbahn, P. E. M.; Nagashima, U.; Wennerberg, J. *J. Am. Chem. Soc.* **1991**, *113*, 424.

(22) (a) Trofimenko, S. *J. Am. Chem. Soc.* **1967**, *89*, 6288. (b) Cotton, F. A.; LaCour, T.; Stanislowski, A. G *J. Am. Chem. Soc.* **1974**, *96*, 754. (c) Crabtree, R. H.; Holt, E. M.; Lavin, M.; Morehouse, S. M. *Inorg. Chem.* **1985**, *24*, 1986. (d) Elschenbroich, C.; Salzer, A. *Organometallics. A Concise Introduction*; VCH: Weinheim, Germany, 1992. (e) Popelier, P. L. A.; Logothetis, G. *J. Organomet. Chem.* **1998**, *555*, 101. (f) Calhorda, M. J. *Chem. Commun.* **2000**, 801. (g) Brookhart, M.; Green, M. L. H.; Wong, L.-L. In *Progress in Inorganic Chemistry*; Lippard, S. J., Ed.; Wiley: New York, 1988; Vol. 36, pp 1−124.

(23) (a) Lehwald, S.; Ibach, H.; Demuth, J. E. *Surf. Sci.* **1978**, *78*, 577. (b) Zecho, Th.; Horn, A.; Biener, J.; Küppers, J. *Surf. Sci.* **1998**, *397*, 108. (c) Haq, S.; King, D. A. *J. Phys. Chem.* **1996**, *100*, 16957.